Investigating MALDI MSI parameters (Part 1) - A systematic survey of the effects of repetition rates up to 20kHz in continuous raster mode

Steven, Rory T; Dexter, Alexander; Bunch, Josephine

DOI:
10.1016/j.ymeth.2016.04.010

Document Version
Peer reviewed version

Citation for published version (Harvard):
Steven, RT, Dexter, A & Bunch, J 2016, 'Investigating MALDI MSI parameters (Part 1) - A systematic survey of the effects of repetition rates up to 20kHz in continuous raster mode', Methods, vol. 104, pp. 101-10. https://doi.org/10.1016/j.ymeth.2016.04.010

A systematic survey of the effects of repetition rates up to 20 kHz in continuous raster mode MALDI MSI

Rory T. Steven[†], Alex Dexter[†,$], Josephine Bunch[†, ‡, *]

[†]: National Centre of Excellence in Mass Spectrometry Imaging (NiCE-MSI), National Physical Laboratory (NPL), Teddington, UK, TW11 0LW

[$]: University of Birmingham, School of Chemistry, B15 2TT

[‡]: School of Pharmacy, University of Nottingham, NG7 2RD

*: Corresponding author: josephine.bunch@npl.co.uk

Abstract

Recent developments in laser performance, combined with the desire for increases in detected ion intensity and throughput, have led to the adoption of high repetition-rate diode-pumped solid-state (DPSS) lasers in matrix assisted laser desorption ionization mass spectrometry imaging (MALDI MSI). Previous studies have demonstrated a more complex relationship between detected ion intensity, stage raster speed and laser pulse repetition rate than the simple linear relationship between number of pulses and detected ion intensity that might be expected. Here we report, for the first time, the interrelated influence of varying laser energy, repetition rate and stage raster speed on detected ion intensity. Thin films of PC 34:1 lipid standard and murine brain tissue with CHCA are analysed by continuous stage raster MALDI MSI. Contrary to previous reports, the optimum laser repetition rate is found to be dependent on both laser energy and stage raster speed and is found to be as high as 20 kHz under some conditions. The effects of different repetition rates and raster speeds are also found to vary for different ion species within MALDI MSI of tissue and so may be significant when either targeting specific molecules or seeking to minimize bias. A clear dependence on time between laser pulses is also observed indicating the underlying mechanisms may be related to on-plate hysteresis-exhibiting processes such as matrix chemical modification.

Introduction

The N_2 laser operating at around 20 Hz was, until relatively recently, standard within UV matrix assisted laser desorption ionisation mass spectrometry (MALDI MS) applications. More recently the desire for improvements in pulse to pulse stability, laser lifetime and repetition rate has led to a widespread uptake in the standard employment by manufacturers of diode pumped solid state (DPSS) lasers. UV DPSS lasers used within MALDI MS are typically variations of neodymium doped lasers including: Nd:YAG,[1-3] Nd:YLF [4, 5] and Nd:YVO_4 [6] with a variety of repetition rate, temporal pulse width and energy characteristics.

The desire for increased laser pulse repetition rate is driven primarily by the need in MALDI MSI for increased throughput when imaging over larger tissue areas or with smaller pixel sizes and is considered to be of great importance for next generation instrumentation. Within MALDI MS it is generally understood that there will be a trade-off between the time spent interrogating a given region and the detected ion intensity achieved for a given analyte of interest; notwithstanding the complete removal of available matrix-analyte crystal in that region. Therefore, the ability to increase the rate of sampling, typically necessitating an increase in repetition rate, is needed.

The benefit of increased repetition rate for faster data acquisition has been demonstrated for spot data acquisition [3, 7] and has also been shown in conjunction with improvements in detected ion intensity over a standard N_2 laser at atmospheric pressure.[8] More recently Bruker Daltonics have developed a new high throughput MALDI ToF imaging platform with a 10 kHz Nd:YAG laser enabling the acquisition of 50 pixels per second. This platform was recently employed to demonstrate the use of low vapour-pressure matrices within high-

vacuum systems for MALDI imaging.[9]

In order to access the fastest image acquisition times it may also be considered necessary to apply these higher repetition rate lasers to MALDI MSI utilising continuous raster mode. This provides throughput benefits over spot mode image acquisition due to the continuous movement of the laser over the sample. The performance of high repetition rate lasers in MALDI MSI in raster mode was the topic of three recent publications.[6, 10, 11] These studies show that higher repetition rate lasers can provide high quality tissue imaging data in short timeframes but also suggest that there is an optimum repetition rate for use in raster imaging below or above which a decrease in detected ion intensity may be observed. An early adoption of a DPSS high repetition rate laser, similar to the one used within this study, was reported by Trim *et al.* where the most effective repetition rates were found to be at around 5 kHz, coinciding with the highest energy-per-pulse emitted by the laser in question [6]. Mass spectra from tissue were also shown within this study using 15 kHz repetition rate which was the highest reported repetition rate used for tissue imaging within MALDI MSI. Interestingly, Spraggins *et al.*, when investigating peptide and CHCA thin films, reported that a reduction in detected ion intensity was observed at higher repetition rates or at lower stage raster speeds, stating that this was due to excessive laser pulse-to-pulse overlap and that a limit of 50 laser pulses per unit area should be observed for optimum performance [10].

Porta *et al.* [12] investigated the effect of altering a number of variables including laser repetition rate between (50 – 1000 Hz) and stage raster speed (1 – 4 mm/s) on quantification in MALDI MS by single reaction monitoring (SRM). Within their work it was observed that an increased ion intensity was observed where faster raster speeds or higher repetition rates were employed.

The interrelated influence of stage raster speed, laser repetition rate and varying laser energy

has never previously been studied, particularly in a tissue imaging context. With the continuing progression of mass spectrometric imaging systems toward high throughput performance, this knowledge is increasingly important to best understand and optimise experiments within MALDI MSI. Within this study, the influence of laser pulsed repetition rate, energy and stage raster speed in continuous stage raster MALDI MSI are studied in both in thin film PC 34:1 lipid standard and CHCA preparations and CHCA coated murine brain tissue sections. For thin film studies the repetition rate is varied between 100 Hz and 20 kHz for stage raster speeds between 0.2 and 2.8 mm/s at four different single pulse energy values between 1.7 and 6.4 μJ. For tissue imaging studies repetition rates of 2 and 20 kHz, raster speeds of 0.5 and 2.8 mm/s and energies of 1 and 3 μJ are assessed.

Methods

Materials

Methanol (HPLC grade) used in preparation of all matrix solutions was purchased from Fisher Scientific (Leicestershire, UK). The water used was purified by an ELGA Purelab Option system (Marlow, UK). Trifluoroacetic acid (TFA, 99.9 % purity) and MALDI matrix α-cyano-4-hydroxycinnamic acid (CHCA, 99 % purity) were purchased from Sigma Aldrich (Dorset, UK). MALDI MS stainless steel imaging plates from Sciex (Ontario, Canada) were used for all experiments. Lipid standard PC 34:1 (18:1 / 16:0) with mass of 759.578 was purchased from Avanti Polar Lipids Incorporated (Delf Zyl, Netherlands).

Tissue Preparation and Sectioning

Mice were sacrificed humanly at the School of Cancer Sciences, University of Birmingham in accordance with the Home Office Animals (Scientific Procedures) Act 1986 [13]. Mouse brain was flash frozen in liquid nitrogen immediately after excision. 4 serial sections at 10 µm thick were collected and thaw mounted onto a single MALDI imaging plate (Sciex). Sectioning was performed on a Leica CM 1850 Cryostat (Milton Keynes, UK).

Matrix Application

For the lipid standard thin film experiments PC 34:1 (0.04 mg mL^{-1} in 80 % CH_3OH) was mixed 1:1 (*v:v)* with CHCA (10 mg mL^{-1} in 80 % CH_3OH, 0.2 % TFA) and for tissue imaging CHCA at 5 mg mL^{-1} in 80 % CH_3OH, 0.1 % TFA was used. A MALDI imaging plate was used in the case of the lipid standard and CHCA thin film. The solution, in either case, was then applied to the imaging plate using a TM Sprayer (HTX Technologies, Carrboro, NC) with a nebuliser temperature of 90 ^{o}C, a solvent flow rate of 0.115 mL/min, a gas pressure of 10 psi, and a spray head speed of 1333 mm min^{-1}. Eight sequential passes across the whole plate were used, each with a spacing of 3 mm between lines, even passes were performed horizontally, and odd passes vertically, and an offset of 1.5 mm was used on passes 3, 4, 7, and 8. This gave a density of matrix and lipid on the plate of 0.115 mg cm^{-2} and 0.0005 mg cm^{-2} respectively resulting in an even distribution of matrix / analyte across the whole plate.

Mass Spectrometry

The laser energy per pulse was measured using a pyro-electric sensor (PD10-C, Ophir Photonics). Further details and a schematic of the laser delivery setup are shown in the supplementary information (SI) Figure S1 and associated text.

MALDI TOF MS analysis was carried out on a QSTAR XL QqTOF instrument using Analyst QS 1.1 with oMALDI server 5.1 (Sciex, Warrington, UK). An Nd:YVO_4 (Elforlight, Daventry, UK: SPOT-10-100-355) DPSS laser with λ = 355 nm, < 40kHz repetition rate and < 1.5 ns pulse length was used in this study. The Nd:YVO_4 laser was continuously triggered by a function generator (TTi – TG2000 20MHz DDS) during all analyses whilst the path of the laser was blocked by a shutter system triggered by the QSTAR oMALDI software to 'turn the laser on and off', rather than triggering the laser directly, ensuring a greater degree of pulse-to-pulse laser stability. The laser was coupled to the MALDI source via a 100 µm core diameter fibre optic patchcord for the tissue imaging experiments (4 meters, Fiberguide Industries via AMS Technologies, Leicestershire, UK, NA = 0.22) and a 105 µm core diameter (Thorlabs, Ltd, NA = 0.22) fibre optic patchcord for the thin film experiments. The raster speeds employed were dictated by the preset software speed values available within the oMALDI (Sciex) software named slowest, slower, slow, medium and fast and correspond to 0.2, 0.3, 0.5, 1.0 or 2.8 mm/s respectively. An *m/z* range of 50 – 1000 was used for all experiments. All data were acquired in positive ion mode.

For the thin film lipid standard analysis the Nd:YVO_4 laser was operated at repetition rates of 100, 500, 1000, 2500, 5000, 7500, 10,000, 12,500, 15,000 and 20,000 Hz at raster speeds of either 0.2, 0.3, 0.5, 1.0 or 2.8 mm/s at a single pulse energies of either 1.7, 2.8, 4.2 or 6.4 µJ. A table of parameter combinations is shown in SI Table S1. The irradiated area on the sample as measured by the fluorometric method [14] was 2.8×10^{-8} m^2 giving fluence values of 225.7, 148.1, 98.8 and 60.0 J/m^2. One raster line of 56 pixels (360 µm diameter per pixel) in length was acquired for each variable combination. The energy of the laser was measured before each of these acquisitions. The average of these values are discussed in the text and used in the fluence calculation.

Tissue image data were acquired at stage speeds of 0.3 and 2.8 mm/s (slower and fast as labelled within the oMALDI software) at repetition rates of 2 and 20 kHz, and energies of 3 and 1 µJ per pulse. The irradiated area on the sample as measured by the fluorometric method [14] was 2.05×10^{-8} m^2 giving fluence values of 146.4 and 48.8 J/m^2. All images were acquired in a random order and each half of the coronal section was acquired separately to provide comparison and control during the course of the experiment. These images were acquired with pixel sizes of 360 µm in x and 50 µm in y and took between approximately 10 and 30 minutes to acquire per section hemisphere.

Processing of MALDI MSI Data

The data were converted from AB Sciex proprietary file format (.wiff) to .mzML using AB MS Data Converter (Sciex, version 1.3) and then converted to imzML using imzMLConverter [15] and processed in MatLab (version R2014b, Math Works Inc, USA). The mean ion counts (peak area) for selected mass-to-charge values were calculated along with the standard deviation and are plotted as mean value ± expanded uncertainty (k = 2, giving a 95 % confidence interval). The image colour scheme was chosen to align with mass spectrometric best practice guidelines.[16] No detector saturation was observed in any data presented within this study. Pulse normalised data were calculated by dividing mean ion intensity values by the number of laser pulses incident per pixel (SI Table S1) for each given variable combination.

Results and Discussion

On the alteration of laser repetition rate in MALDI MS relevant lasers

The use of DPSS lasers is now common within the field of MALDI MS and MSI. In the majority of cases these lasers will be embedded within commercially supplied mass spectrometry instrumentation and therefore, inaccessible to the user beyond the minimal control given within the software. When the operational repetition rate of the laser is altered, the energy per pulse emitted by the laser may vary depending upon the triggering frequency (repetition rate). This may be due to thermal equilibration phenomenon or lasing material excited state lifetime related effects, for example. In addition, a phenomenon called 'spiking' may occur, depending upon the laser design, whereby the first number of triggered laser pulses, after a longer period without triggering, will have significantly higher energy until a steady state is reached. This phenomena could be present at the initiation of laser sampling of each pixel or raster line within a MALDI MS experiment. A shutter triggering system was used within this study to help ensure the absence of these and other laser instabilities. A manuscript on the use of a shuttered triggering system within MALDI MS is currently in preparation. The energy output from the laser over the relevant range of repetition rates used within this study is shown in Figure 1. The repetition rate at which the highest output energy is emitted is observed to be in the region of ~ 3 to 6 kHz.

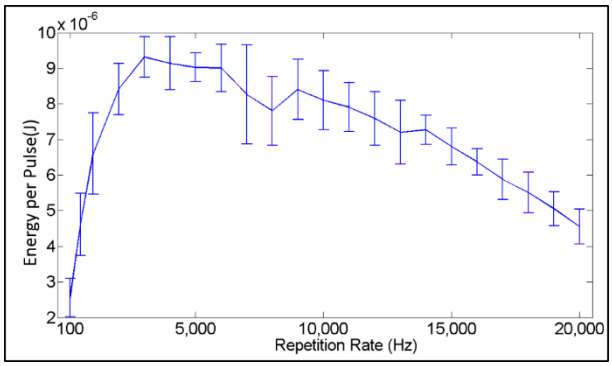

Figure 1. Energyoutput (mean ± 1 standard deviation) of laser over experimental range of repetition rates without any alteration in the level of attenuation.

In order to better study the influence of repetition rate within MALDI MSI this changing energy with repetition rate needs to be accounted for. Typical commercial MALDI MSI instruments do not enable energy measurement or uninhibited control of repetition rate. Therefore, we implemented an improved laser delivery system to enable on-line energy monitoring and control, thus allowing the attenuation to be altered so that a constant energy was delivered to the sample regardless of the repetition rate employed. A schematic of this setup is shown in SI Figure S1.

Variation of Repetition Rate and Raster Speed in Continuous Raster Sampling MALDI MS

To study the interrelating influences of laser repetition rate, energy and stage raster speed a thin film sample of CHCA and lipid standard PC 34:1 was interrogated in continuous raster sampling mode. The ion intensities for the three detected intact adducts ($[M+H]^+$, $[M+Na]^+$ and $[M+K]^+$) of PC 34:1 were summed and the results for raster speeds of 0.2, 0.5, 1.0 and 2.8 mm/s are shown below in Figure 2. These three adducts were combined in this way to account for any change in ratio of these species over the experimental range of variables. The equivalent graph for the 0.3 mm/s raster speed, omitted from Figure 1, is shown in SI Figure S2.

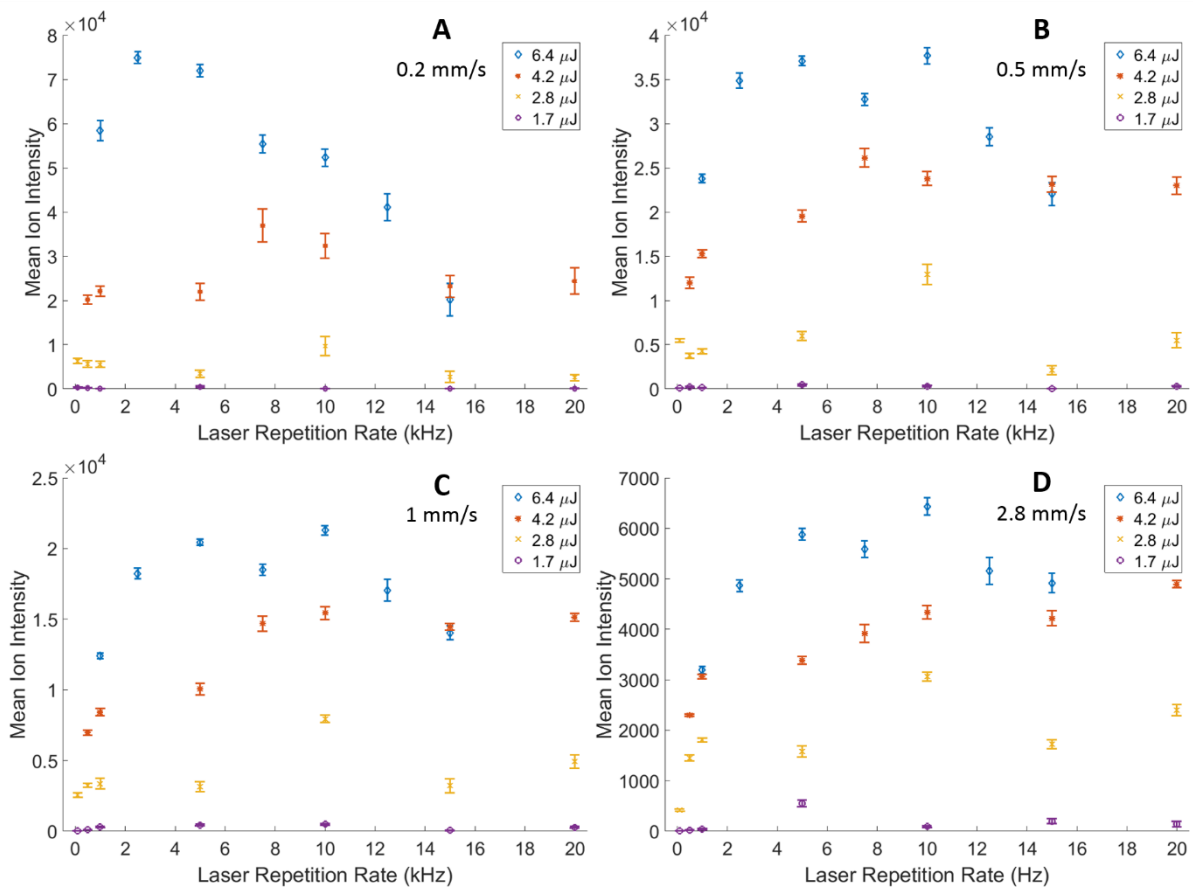

Figure 2. Mean detected ion intensity per pixel for sum of intact adducts of PC 34:1 lipid standard $[M+H]^+$, $[M+Na]^+$, $[M+K]^+$ with varying repetition, energy and raster speed. Energies of 6.4, 4.2, 2.8 and 1.7 µJ at a range of laser pulse repetition rates from 100 to 20,000 at raster speeds of: A – .0.2 mm/s, B – 0.5 mm/s, C – 1 mm/s, D – 2.8 mm/s. Errors are expressed as k = 2 expanded uncertainty giving a 95 % confidence interval.

A number of broad trends are evident within these data. Firstly, the detected ion intensity clearly increases with increasing fluence as a global trend, an observation that is in agreement with other research.[17, 18] The highest ion intensities were detected at 0.2 mm/s, 2.5 kHz and 6.4 µJ. However, the impact of changing fluence varies dramatically depending upon the

chosen repetition rate and raster speed employed. For example, at 500 Hz, 0.2 mm/s, 6.4 and 4.2 µJ (Figure 2 – A) there is a marked difference in the detected intact lipid ion intensity. However, at 15 kHz with the same speed there is little difference between the detected ion intensity at these two energies. Similar observations are also evident across the raster speeds investigated whereby the differences in the detected ion intensity at different energies (and so fluences) are enhanced or reduced depending upon the laser repetition rate. Secondly, the relationship between detected ion intensity and repetition rate, for a given raster speed, is dependent upon the laser energy employed. For example, at 0.2 mm/s raster speed the optimum repetition rate is 2.5 kHz for 6.4 µJ, whereas it is 7.5 kHz for 4.2 µJ and 10 kHz at 2.8 µJ (Figure 2 – A), a shift to higher optimum repetition rates with decreasing energy. This shift of optimum repetition rate across energies is evident across the different raster speeds e.g. at 2.8 mm/s the 6.4 µJ data shows an optimum repetition rate at 10 kHz whereas the 4.2 µJ data arguably shows an optimum at 20 kHz. Thirdly, the optimum repetition rate for a given energy broadly follows an upward trend where the raster speed increases and / or the energy decreases. For example, the 6.4 µJ data shows an optimum repetition rate of 2.5 kHz at 0.2 mm/s whereas it is 10 kHz at 2.8 mm/s and for the 4.2 µJ data the optimum repetition rate is 7.5 kHz at 0.2 mm/s whereas it is 20 kHz at 2.8 mm/s. Finally, the above discussed trends appear to be less evident as the energy is decreased i.e. the impact of repetition rate at a given raster speed is considerably lessened at lower energies and at the lowest energies within Figure 2 the repetition rate used results in little difference. Re-arranged bar chart versions of these same data are shown in SI Figure S3. In addition to the summed intact lipid ions shown in Figure 2, the total ion counts (TIC) per pixel were plotted in the same manner as was the TIC normalised version of Figure 2 (SI Figures S4 and S5). Further to the extracted ion intensity data the spectral information also provides additional perspective on the

relationship between energy, stage raster speed and laser pulse repetition rate. Example mean spectra for some pertinent variable combinations are displayed within Figure 3.

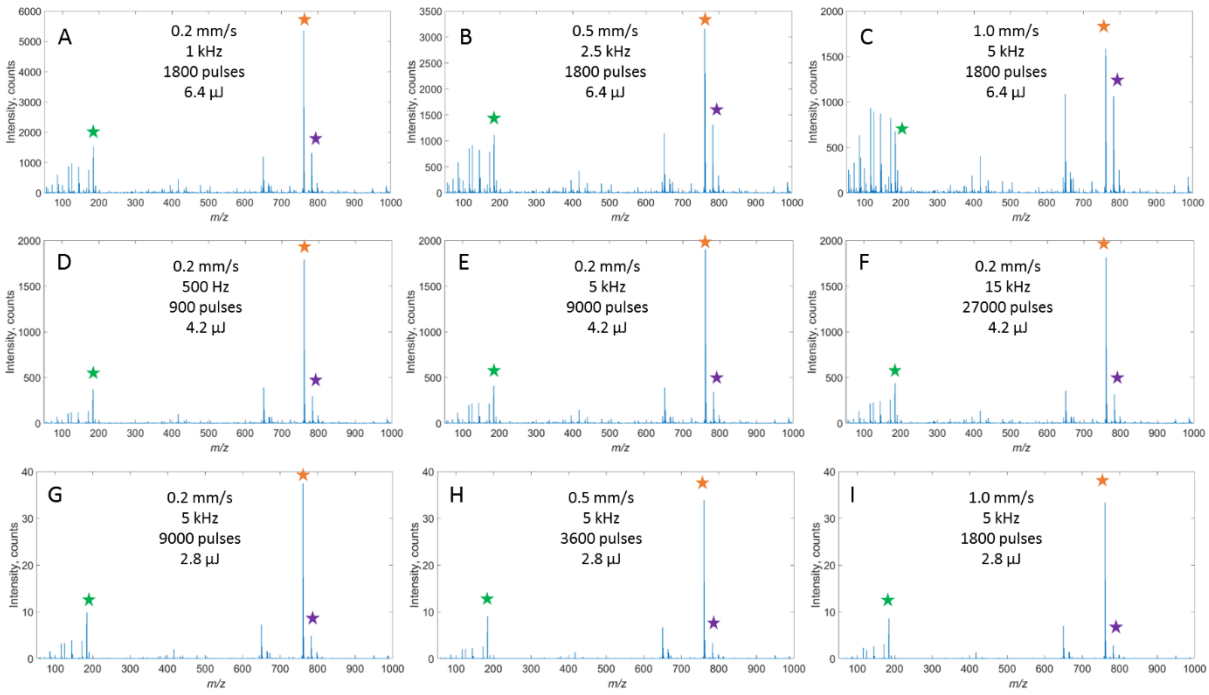

Figure 3. Example mean spectra from thin film lipid standard and CHCA acquired with varying laser repetition rate, energy and stage raster speed from the data shown in Figure 2. The green star (left), orange star (middle) and purple star (right) in each spectra indicate peaks at *m/z* = 184.1, 760.6 and 782.6 respectively.

The alteration of repetition rate and raster speed across several pulse energies provides the opportunity to compare data from pixels which have received the same number of pulses but at different temporal rates. Each pixel within the data acquired at 6.4 µJ with raster speed and repetition rate of 0.2 mm/s and 1 kHz, 0.5 mm/s and 2.5 kHz or 1 mm/s and 5 kHz all received 1800 pulses per pixel at this same fixed energy. The mean spectra from these

respective experiments are shown in Figure 3 A, B and C. It is clear that despite the same number of pulses at the same energy there is an increase in detection of the protonated PC 34:1 lipid ion ($[M+H]^+$ at *m/z* = 760.6) with decreasing raster speed and repetition rate. In addition, the intensity of the sodiated ion ($[M+Na]^+$ at *m/z* = 782.6) and the phospholipid head-group fragment ion at *m/z* = 184.1 [19] (proposed structure for these and other fragment ions shown in SI Figure S10) increase relative to the $[M+H]^+$ peak as the raster speed and repetition rate are increased (Figure 3, A – C). Graphs displaying these changes across all variable combinations for *m/z* = 184.1 are displayed in SI Figure S7. Further, the (lack of) influence of increased pulses per pixel (under certain circumstances) due to increasing repetition rate are shown in Figure 3 D – F where increasing repetition rate (and so pulses per pixel), at a fixed energy, appears to have little significant effect on the intensity of peaks within the detected mass spectra. Additionally, at lower energies, the raster speed employed (and again the number of pulses per pixel) at a fixed energy and repetition rate may have little influence over the detection ion intensity and spectral profile (Figure 3, G – I).

The number of pulses per pixel, whilst not causing linear variation in the detected ion intensities, can be used to normalize the data displayed within Figure 2. Graphs showing these normalised data are shown in Figure 4.

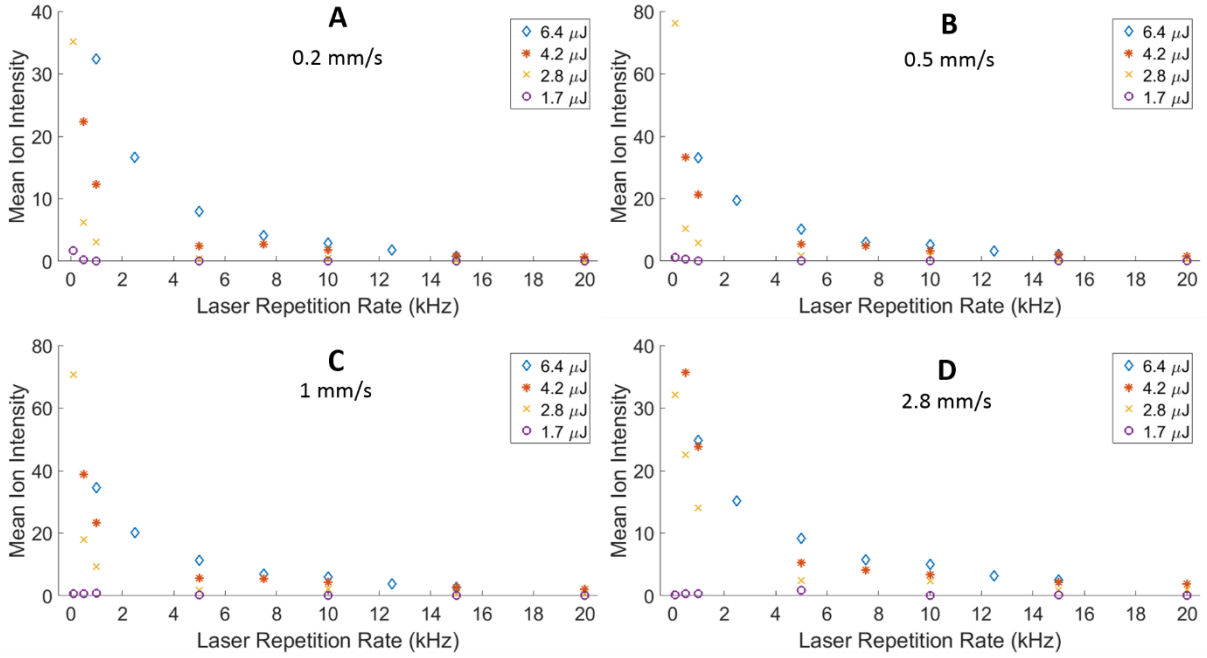

Figure 4. Mean ion intensity per-pixel per-laser-pulse. Data displayed within Figure 2 divided by the number of laser pulses incident per pixel for each given variable combination. An increase in average detected ion intensity per-pixel, per-laser-pulse, is observed with decreasing laser repetition rate.

In all cases, for a given energy, the lower the repetition rate used, a trend towards a higher detected ion intensity per-pixel, per-laser-pulse, is observed. This may be related to the fact that the time period between laser pulses increases with decreasing repetition rate and so, for a specific stage speed, the area of sample irradiated by each new laser pulse will also increase. This increasing area of fresh sample irradiated by each new laser pulse is not, however, the sole reason for the trends seen within Figures 2, 3 and 4. For example, the pulse normalized data show similar ion intensity per-pixel per-laser pulse across all raster speeds investigated (Figure 4). Additionally, the trends between each energy data-set alter across the different raster speeds, whereby, the difference between detected ion intensity per-pixel per-

laser-pulse, at each laser energy, reduces as the raster speed increases. This is particularly evident at the lower repetition rates e.g. at 0.2 mm/s and 1 kHz the ion intensity at 6.4 μJ is ~ 3 times that of 4.2 μJ; this ratio then decreases to ~ 3 at 0.5 and 1 mm/s and further decreases a roughly equal value at 2.8 mm/s (Figure 4). The changing trends of the pulse normalized data at different energies are further exemplified when displayed as graphs of single energy data as oppose to the single raster speed data shown above (SI Figure S6). Here the changing trends at different energies can clearly be seen across the varying raster speeds, for a given energy.

The change in ratio of ions detected at *m/z* = 760.6 with ions detected at *m/z* = 782.6 or 184.1 can also be illustrated by plotting these ratios in the same form as Figure 2. These ratio graphs for $[M+H]^+/[M+Na]^+$ are displayed in SI Figure S9 and those for $[M+H]^+$/ *m/z* = 184.1 in SI Figure S8. Evident within these figures is: the decreasing ratio for $[M+H]^+/[M+Na]^+$ with increasing energy across all raster speeds; across almost all energies and raster speeds aside from 2.8 mm/s and 1.7 μJ the $[M+H]^+/[M+Na]^+$ ratio also generally decreases with increasing repetition rate until some minima at which the ratio increases again, for a given raster speed and energy. For the ratio of $[M+H]^+$ to the ion detected at *m/z* = 184.1 the variation is less significant but there is again a reduction in this ratio with increasing energy.

In summary, the major trends observed within these analyses are: the optimum repetition rate for increased detected ion intensity varies considerably depending upon the stage raster speed and laser energy used within the experiment; there are differential effects on different detected ions as a result of varying laser repetition rate, fluence and stage raster speed; there is a clear dependence of detected ion intensity on the time period between incident laser

pulses where the same number of laser pulses are incident per pixel under different raster speed and repetition rate combinations (Figure 3 A – C).

It is worth, at this point, commenting briefly on the workings of the mass spectrometer used within this study, though far more detailed descriptions are available [20]. The QSTAR XL instrument is a quadrupole time-of-flight instrument which, in single MS mode (full mass range ToF analysis), operates the quadrupoles as ion guides only. Consequently the collisional cooling of the ions, at the repetition rates employed within this study, will result in a quasi-continuous beam of ions through the quadrupole regions to the ToF pusher region. Consequently the mass spectrum recorded for each pixel is the sum of hundreds or thousands of ToF cycles (depending upon the pixel acquisition time) – the ToF effectively samples from this continuous beam of ions. As the mass range is fixed within this study, the ToF pusher frequency is also fixed. Therefore, the number of ToF cycles summed on average for the ions resulting from one laser pulse will vary, depending upon the repetition rate. One can further normalise the data shown in Figure 4 to the number of ToF cycles, resulting in values of mean ions per laser pulse, per ToF cycle. However, as the number of ToF cycles per laser pulse is inversely proportional to the laser repetition rate used, the trends seen simply revert back to the exact shapes seen in Figure 2 with an associated scaling of the y-axis.

Variation of Repetition Rate and Raster Speed in Continuous Raster Sampling MALDI MS Imaging of Murine Brain Tissue

The complex interrelation of spectral information as a result of varying laser energy, repetition rate and stage raster speed for the analysis of thin-film lipid standard and CHCA

strongly implies that these variables will also show complex interrelated behavior when investigated in the context of MALDI MSI analysis. Continuous stage raster MALDI MS imaging data at 0.3 and 2.8 mm/s, 2 and 20 kHz and 1 and 3 µJ were acquired from eight serial sections of murine brain tissue. Image data were acquired in a random order from section hemispheres. The corresponding hemispheres from a single brain section were analysed with a single set of variables but at different time points to act as an internal temporal control. Selected ion images and mean on-tissue spectra from these analyses are shown in Figures 5 and 6. Detected peaks, tentatively assigned from literature, corresponding to PC 16:0/16:0 $[M+K]^+$ at *m/z* = 772.5, PC 18:0/18:1 $[M+K]^+$ at *m/z* = 826.6, unknown tissue related molecule at *m/z* = 868.5 (tentative assignment of PI 37:6, PA 35:2 or DG 42:11 based on Lipid Maps database search, the lower mass resolving power of this instrument prevents a more accurate match) and the PC lipid head-group fragment at *m/z* = 184.1.[21-23]

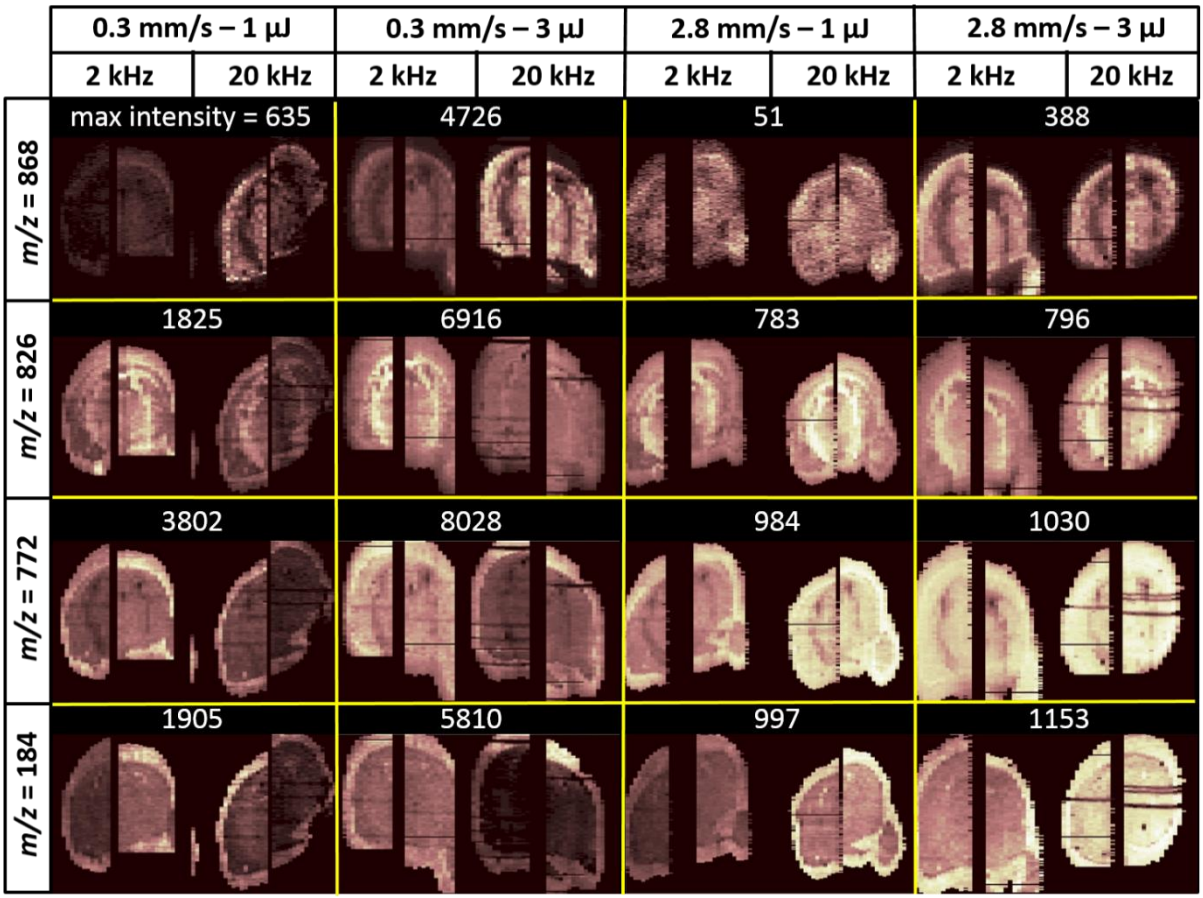

Figure 5. Selected ion intensity images from murine brain tissue sections for varying laser energy per pulse, pulse repetition rate and stage raster speed. Columns of single ion images are shown from the same tissue section. Each pair of single ion images at a given raster speed and energy are on the same intensity scale and the maximum ion intensity of this scale is displayed as a number above the corresponding pair. Intensity scales progress from low to high intensity. The low intensity raster lines (dark rows of pixels) are areas where the laser triggering did not activate during data acquisition.

As was observed from analysis of thin films, the analyses at the slower raster speed and higher energy give the highest detected ion intensities for intact lipid species (Figure 5, 0.3 mm/s, 3 µJ, 2 and 20 kHz). Despite this energy and raster speed clearly giving the highest detected ion

intensities, the optimum repetition rate appears to vary depending upon the peak chosen for display where, in this example, 20 kHz is more appropriate for the ion at *m/z* = 868.5 but 2 kHz shows higher intensity for *m/z* = 826.6, 772.5 and 184.1. This phenomena of differential optimum repetition rate is also evident in the 1 μJ, 0.3 mm/s data set but is not evident in quite the same way for the 2.8 mm/s data, where there is either little difference between the 2 and 20 kHz data or 20 kHz is slightly more optimal overall. This echoes the findings for the high raster speed data acquisition in the thin-film samples discussed above, where the impact of repetition rate decreased as the raster speed is increased with a general trend to higher optimum repetition rates at certain energies.

In all cases the detected ion intensities are higher for the higher laser energy, an observation that would likely be expected based upon existing literature but one which has not been studied within the context of MALDI MS imaging studies before. It is clear from several of the images that there is a noticeable degree of leeching of endogenous molecules from the tissue, a result of the slightly overly 'wet' sample preparation employed, creating the halo effect observed before in the literature and is particularly evident for the *m/z* = 184.[21] This is not an issue for the conclusions presented in this study and can even be considered useful with regards to providing insight into the effects of repetition rate, energy and stage raster speed. Foremost, the relative levels of fragmentation on tissue and in the halo vary depending upon the energy, repetition rate and raster speed. Typically an increase in fragmentation, for a given laser energy, is to be expected in the halo due to the lower energy requirement for desorption / ionization from stainless steel as compared to the tissue surface. Though, it is also possible that already formed PC headgroup fragments are preferentially solubilized and therefore leached from the tissue, causing a similar visible effect. This is clear from Figure 5 in all cases apart from at 2.8 mm/s, 3 μJ and 20 kHz where the level of fragmentation on tissue

is approximately equal to that of the halo region. These and other trends observed within this tissue image data set are evident within the mean on-tissue spectra shown within Figure 6.

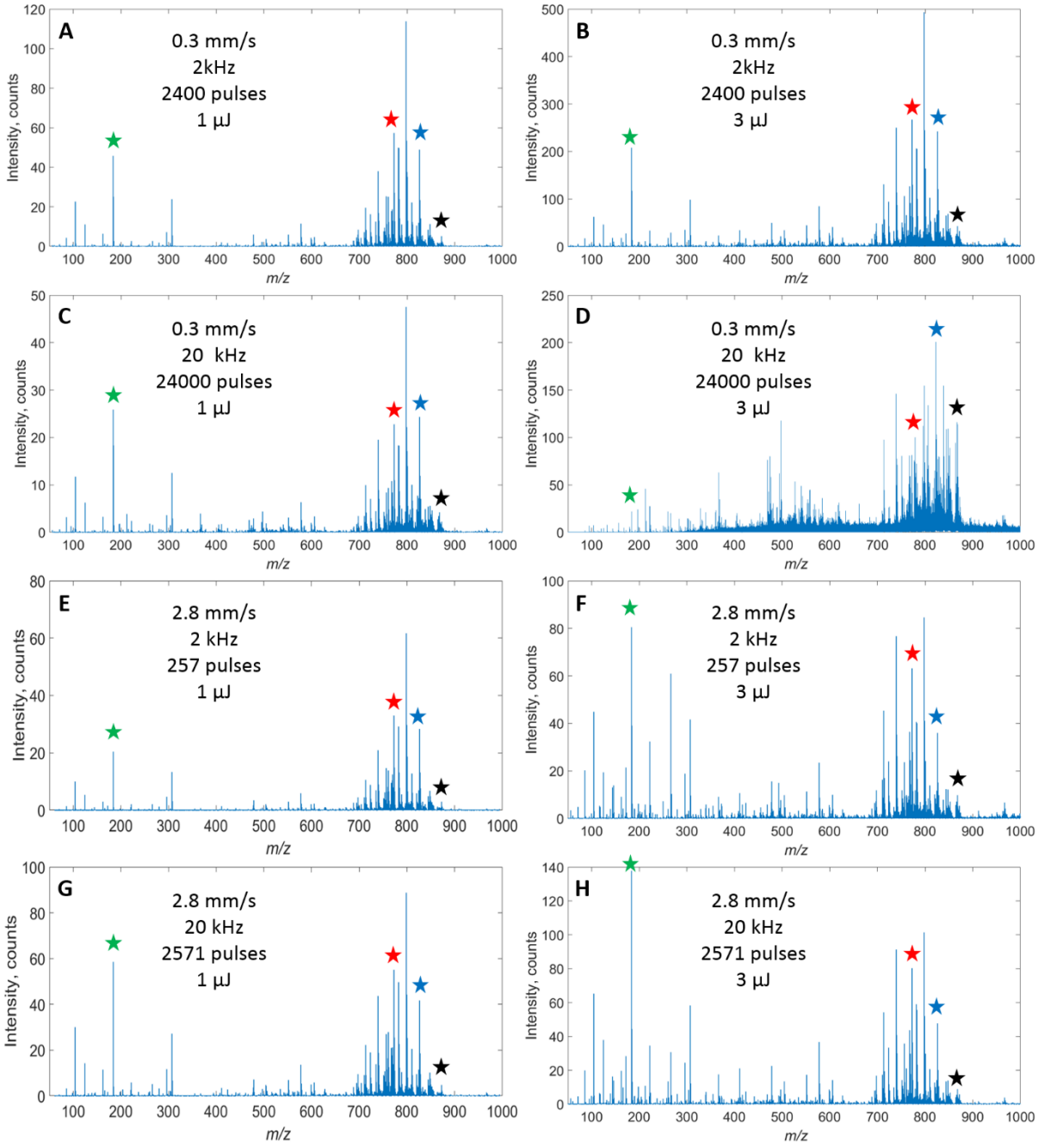

Figure 6. Mean on-tissue spectra from murine brain tissue acquired with varying laser repetition rate, energy and stage raster speed from data shown in Figure 4. The green star (left side on each spectrum), red star (left middle), blues star (right middle) and black star

(right) in each spectra indicate peaks shown as images in Figure 4 at *m/z* = 184.1, 772.5 and 826.6 and 868.5 respectively.

The general optimum ion intensity at 0.3 mm/s, 2 kHz and 3 μJ is again evident within Figure 6 B but it remains clear that the higher repetition rate (20 kHz) data can provide an increased detected ion intensity for some peaks observed in the mass spectrum (Figure 6 D). For example the peak at *m/z* 868.5 is more intense in Figure 6 D as compared to 6 B. Further MS/MS studies are required to better assign these enhanced ions. Also clear within the spectra is the large increase in intensity for the peak at *m/z* = 184.1 (likely PC lipid head-group fragment [19]) relative to the mostly intact lipid species detected within the *m/z* = 700 – 900 region in the high energy, high raster speed data shown in Figure 6 F and H. Despite this the highest intensity detected for *m/z* = 184.1 is observed at 0.3 mm/s and 2 kHz (Figure 6 B) where it has increased in line with a global ion intensity increase rather than relative to intact lipid peaks. In addition to this relative increase of *m/z* = 184 in Figure 6 F and H, there is also an increase in other lipid fragment and matrix related ions below *m/z* = 600 relative to the intensity of the intact species when compared to the other spectra. The spectrum which stands out the most is Figure 6 D where, as well as the above mentioned increase in detected ion intensity for a number of peaks, there is also an almost global increase in the detected ion intensity for typically low intensity peaks throughout the majority of the mass spectrum above *m/z* = 300. The display of this spectrum in Figure 6 D initially gives the impression that an increase in noise baseline is observed using these laser parameters but this is not, in fact, the case and when zooming in to view smaller *m/z* regions within this spectrum one can see this is actually an increase in fully resolved low intensity peaks compared to the other spectra (see

SI Figure S11 and S12 for zoomed regions of spectra shown in Figure 6 D and B respectively). More work is, however, required to confirm whether these ions are intact species detected with a greater intensity or the result of other processes such as changing adduct formation or increased ion fragmentation and meta-stable decay, for example.

Again, the trends observed within the data presented can be summarized as follows: the optimum repetition rate for highest detected ion intensity depends upon the stage speed and laser energy used, with increasing benefit of higher repetition rates evident at higher raster speeds and lower energies. The extent to which these variables enhance the detection of a specific ion depend upon the ion in question and this must be considered in targeted analysis to select variables most appropriate but should also be considered in un-targeted experiments where effects may be more severe for some ions and not uniform over the spectral range. There is also a clear dependence of detected ion intensity on the time period between incident laser pulses where the same or very similar numbers of laser pulses are incident per pixel at different repetition rate and raster speed combinations (Figure 3 A – C and Figure 6 B and H).

Although the trends observed from analysis of lipid standard and tissue (Figures 2 – 6) provide strong evidence that the relationship between fluence, raster speed and repetition rate is highly complex, and serve to direct researchers seeking to optimise their experiments, they do not in themselves reveal the underlying mechanisms causing these phenomena. Changing intensity of different lipid peaks in MALDI MSI of tissue, changing intensity of lipid adduction and alteration of fragmentation levels are evident but do not appear to be the primary cause of the observed trends, though these two phenomena are likely products of the underlying mechanism(s).

Research on the variation of raster speed and repetition rate by *Spraggins et al.* showed a decrease in ion yield when approximately 50 pulses per unit area were exceeded [10]. Whilst this study does, in places, broadly support their conclusions, only in the minority of cases here were less than 50 pulses per unit area employed and in most cases this number was vastly exceeded (SI Table S1). At all lower fluences, repetition rates of above 5 kHz were often found to be optimum and higher repetition rates as well as higher raster speeds were also often found to be beneficial. This suggests the picture is more complex than a simple pulse per unit area limit above which performance is reduced.

Investigations by *Fournier et al.* in a single large protein doped sinapinic acid (SA) crystal revealed pulse number and energy related effects on detected ion intensity [24]. Ion yield per pulse was observed to halt after ~ 30 pulses at energy of 1.5 – 2 µJ but several 8 – 9 µJ pulses allowed further ion acquisition at the lower energy again. Structural changes to the crater surface, as well as decarboxylation of the matrix and the effect of this on the UV absorption were thought to be the cause; it was further mentioned that a similar effect was also observed in CHCA [24]. Aspects of this phenomena were further investigated by Tarzi et al. who studied the effects of heating on various UV MALDI MS matrices [25]. It was shown that heating of CHCA and SA led to chemical changes in the matrix. Decarboxylation of these matrices was again found to be present though to a much greater extent in CHCA than in SA. It was proposed that the observed thermochemical degradation of SA and CHCA was likely to blame for the phenomena seen by *Fournier et al* [24, 26]. Qiao *et al.* investigated issues relating to number of laser pulses and fluence for spot mode analysis using Nd:YAG and N_2 lasers [27]. They found that the ion yield of substance P (1347 Da) with CHCA matrix at 560 J m^{-2} reached its maximum of ~ 1.4×10^4 after ~ 150 laser pulses and the sample was visibly depleted. At 320 J m^{-2} the maximum ion yield of ~ 4×10^4 was reached after ~ 300 laser pulses but there was no

accompanying visible depletion of the sample. It was suggested that the decay of the ion signal at lower fluences, despite the remaining visible sample, could be due to surface modification / heating / hysteresis effects [24, 26, 28]. Recently, Wiegelmann *et al.* observed similar phenomena when studying detected ion intensity at various laser wavelengths for CHCA, di-hidroyxybenzoic acid (DHB) and Fluorinated and Chlorinated CHCA derivatives (DiFCCA and CLCCA) [29]. The ion intensity per laser pulse for 900 successive pulses showed an initial increase followed by a subsequent decrease, where it was stated that changes in the optical absorption profile of pre-irradiated matrix layers could be responsible for this overall chromatogram shape.

Evidence obtained by the Zenobi group [30], amongst others, shows that matrices such as 2,5 DHB and nicotinic acid, will experience temperatures as high as 1000 K during MALDI MS analyses. Furthermore, matrix dimerization was observed in CHCA crystals for up to several hours after laser irradiation and the dynamics of this formation process were observed to depend upon crystal morphological properties and the laser energy [31]. Additionally, it is known in certain laser ablation scenarios that the threshold fluence of ablation can have a dependence on the laser repetition rate due to accumulation of thermal energy on these timescales [32].

The above mentioned phenomena may help to explain the trends observed within this study. The apparent influence of pulse-to-pulse delay and stage movement under the laser imply that phenomena occurring on the plate, on timescales of ~ 10^{-5} to 0.01 seconds or longer, are potential causes of the observed trends. Therefore, the structural modifications observed by Fournier *et. al*, the deposition and subsequent dissipation of thermal energy and dimerization (or even multimerization) could all contribute to these observations. For example, a

decreased pulse-to-pulse delay time would potentially result in an increase in local temperature on average, altering the morphology of the sample left behind on the sample plate and causing further decarboxylation of this matrix material and differing dimerization properties. Consequently the material ablated by subsequent laser pulses would exhibit different mass spectral properties to those acquired under a different repetition rate. As the stage speed dictates the number of laser pulses incident on a particular area this rationale also covers the alteration of raster speed and its effect upon the mass spectra observed within this study.

It is worth noting that due to the variation of photon density across the laser beam profile used in this study, there may be similar low / high energy variation analogous to that to that used by *Fournier et al.* and so varying surface modification and hysteresis effects may well be occurring naturally within this and other MALDI MSI studies for this reason also.

This implies that very different relationships between laser energy, repetition rate and stage raster speed would be observed if similar studies to this were carried out with other matrices and possibly even with different sample preparations of the same matrix where crystal size and morphology differ substantially. Matrices observed by Fournier and Tarzi not to undergo these same decarboxylation effects would perhaps exhibit a more linear trend between the number of laser pulses per pixel and the detected ion intensity. Also matrices which undergo some other form of chemical or structural modification during MALDI MS analysis should exhibit some other trend depending upon the repetition rate, raster speed and energy used.

Conclusions

Here a high repetition rate (≤ 20 kHz; Nd:YVO_4) laser was used in conjunction with a hybrid orthogonal MALDI QqToF mass spectrometer to probe the relationship between beam profile, repetition rate, raster speed and fluence within raster mode MSI of lipids.

Analysis of thin layer CHCA and lipid standard preparations show complex relationships with several underlying trends evident within the data. Similarly complex relationships are also shown to be present in tissue data sets. A fluence dependence of the relationship between repetition rate and raster speed was shown. Repetition rates of 20 kHz were, for the first time within MALDI MSI, employed to acquire tissue image data and were observed to provide optimum ion yield under certain scenarios in tissue with continuous raster mode analysis.

This study provides new and detailed information into the interplay of these important variables within MALDI MSI studies. Particularly with regards to the differential detection of certain lipid species, ion adduct variation and fragmentation processes at different repetition rates and the dependence of MS data of the pulse-to-pulse delay time. Though these features are not the sole causes of the observed trends they are instead likely to be symptoms of on-plate thermally-driven hysteresis-exhibiting processes such as matrix chemical and structural modification as well as sample heating. The extent to which this is the case is not totally clear, however, and further work investigating these phenomena in other matrix – sample systems is required to further elucidate this issue.

The influence of both repetition rate and raster speed are shown to be extremely important when optimizing raster imaging experiments for increased detected ion intensity and or throughput. These considerations are also crucial for the improved understanding and implementation of high repetition rate lasers, high throughput and high ion yield MALDI MS imaging. Once the operator or experimenter understands the role these variables play in

influencing the detected ion intensity of MALDI MS, this knowledge can be implemented in applications such as tissue imaging. In addition, a better understanding of these variables allow one to move their investigations into other important areas of MALDI MS, such as studying the influence of new matrices, with a better overall understanding of the influence of these variables on the data obtained.

Acknowledgements

Thanks to Keith Oakes for useful discussion. Funding was provided by NPL strategic research program 'NiCE MSI' project SR 116301 and Innovate UK (formerly TSB) award 101788. AD is in receipt of an EPSRC studentship via the PSIBS doctoral training centre (EP/F50053X/1), in collaboration with AstraZeneca and the National Physical Laboratory.

References

1. N. Zaima, T. Sasaki, H. Tanaka, X.W. Cheng, K. Onoue, T. Hayasaka, et al., Imaging mass spectrometry-based histopathologic examination of atherosclerotic lesions, Atherosclerosis. **217** (2011) 427-432.
2. G.A. Amadei, C.F. Cho, J.D. Lewis, L.G. Luyt, A fast, reproducible and low cost method for sequence deconvolution of 'on bead'peptides via 'on target'maldi TOF/TOF mass spectrometry, J Mass Spectrom. **45** (2010) 241-251.
3. J.J. Corr, P. Kovarik, B.B. Schneider, J. Hendrikse, A. Loboda, T.R. Covey, Design considerations for high speed quantitative mass spectrometry with MALDI ionization, J Am Soc Mass Spectr. **17** (2006) 1129-1141.
4. S.N. Jackson, B. Colsch, T. Egan, E.K. Lewis, J.A. Schultz, A.S. Woods, Gangliosides' analysis by MALDI-ion mobility MS, Analyst. **136** (2010) 463-466.
5. S. Sundarapandian, J.C. May, J.A. McLean, Dual Source Ion Mobility-Mass Spectrometer for Direct Comparison of Electrospray Ionization and MALDI Collision Cross Section Measurements, Anal Chem. **82** (2010) 3247-3254.
6. M.R. Clench, P.J. Trim, M.C. Djidja, S.J. Atkinson, K. Oakes, L.M. Cole, et al., Introduction of a 20 kHz Nd:YVO4 laser into a hybrid quadrupole time-of-flight mass spectrometer for MALDI-MS imaging, Anal Bioanal Chem. **397** (2010) 3409-3419.
7. E. Moskovets, J. Preisler, H.S. Chen, T. Rejtar, V. Andreev, B.L. Karger, High-throughput axial MALDI-TOF MS using a 2-kHz repetition rate laser, Anal Chem. **78** (2006) 912-919.
8. J.A. McLean, W.K. Russell, D.H. Russell, A high repetition rate (1 kHz) microcrystal laser for high throughput atmospheric pressure MALDI-quadrupole-time-of-flight mass spectrometry, Anal Chem. **75** (2003) 648-654.
9. N. Ogrinc Potočnik, T. Porta, M. Becker, R. Heeren, S.R. Ellis, Use of advantageous, volatile matrices enabled by next-generation high-speed matrix-assisted laser desorption/ionization time-of-flight imaging employing a scanning laser beam, Rapid Commun Mass Sp. **29** (2015) 2195-2203.

10. R. Caprioli, J.M. Spraggins, High-Speed MALDI-TOF Imaging Mass Spectrometry: Rapid Ion Image Acquisition and Considerations for Next Generation Instrumentation, J Am Soc Mass Spectr. **22** (2011) 1022-1031.
11. B.M. Prentice, C.W. Chumbley, R.M. Caprioli, High-speed MALDI MS/MS imaging mass spectrometry using continuous raster sampling, J Mass Spectrom. **50** (2015) 703-710.
12. T. Porta, A. Lesur, E. Varesio, G. Hopfgartner, Quantification in MALDI-MS imaging: what can we learn from MALDI-selected reaction monitoring and what can we expect for imaging?, Anal Bioanal Chem. **407** (2015) 2177-2187.
13. C. Hollands, The Animals (scientific procedures) Act 1986, The Lancet. **328** (1986) 32-33.
14. R.T. Steven, A.D. Palmer, J. Bunch, Fluorometric Beam Profiling of UV MALDI Lasers, J Am Soc Mass Spectr. **24** (2013) 1146-1152.
15. A.M. Race, I.B. Styles, J. Bunch, Inclusive sharing of mass spectrometry imaging data requires a converter for all, Journal of Proteomics. **75** (2012) 5111-5112.
16. A.M. Race, J. Bunch, Optimisation of colour schemes to accurately display mass spectrometry imaging data based on human colour perception, Anal Bioanal Chem. **407** (2015) 2047-2054.
17. K. Dreisewerd, The desorption process in MALDI, Chem Rev. **103** (2003) 395-425.
18. J. Soltwisch, T.W. Jaskolla, F. Hillenkamp, M. Karas, K. Dreisewerd, Ion yields in UV-MALDI mass spectrometry as a function of excitation laser wavelength and optical and physico-chemical properties of classical and halogen-substituted MALDI matrixes, Anal Chem. **84** (2012) 6567-6576.
19. R.T. Steven, J. Bunch, Repeat MALDI MS imaging of a single tissue section using multiple matrices and tissue washes, Anal Bioanal Chem. **405** (2013) 4719-4728.
20. I.V. Chernushevich, A.V. Loboda, B.A. Thomson, An introduction to quadrupole–time-of-flight mass spectrometry, J Mass Spectrom. **36** (2001) 849-865.
21. R.T. Steven, A.M. Race, J. Bunch, Para-Nitroaniline is a promising matrix for MALDI-MS imaging on intermediate pressure MS systems, J Am Soc Mass Spectr. **24** (2013) 801-804.
22. H.Y.J. Wang, C.B. Liu, H.W. Wu, J.S. Kuo, Direct profiling of phospholipids and lysophospholipids in rat brain sections after ischemic stroke, Rapid Commun Mass Sp. **24** (2010) 2057-2064.
23. K. Shrivas, T. Hayasaka, N. Goto-Inoue, Y. Sugiura, N. Zaima, M. Setou, Ionic matrix for enhanced MALDI imaging mass spectrometry for identification of phospholipids in mouse liver and cerebellum tissue sections, Anal Chem. **82** (2010) 8800-8806.
24. I. Fournier, J.C. Tabet, G. Bolbach, Irradiation effects in MALDI and surface modifications - Part I: Sinapinic acid monocrystals, Int J Mass Spectrom. **219** (2002) 515-523.
25. O.I. Tarzi, H. Nonami, R. Erra-Balsells, The effect of temperature on the stability of compounds used as UV-MALDI-MS matrix: 2, 5-dihydroxybenzoic acid, 2, 4, 6-trihydroxyacetophenone, α-cyano-4-hydroxycinnamic acid, 3, 5-dimethoxy-4-hydroxycinnamic acid, nor-harmane and harmane, J Mass Spectrom. **44** (2009) 260-277.
26. I. Fournier, R. Beavis, J. Blais, J. Tabet, G. Bolbach, Hysteresis effects observed in MALDI using oriented, protein-doped matrix crystals, International journal of mass spectrometry and ion processes. **169** (1997) 19-29.
27. H. Qiao, V. Spicer, W. Ens, The effect of laser profile, fluence, and spot size on sensitivity in orthogonal-injection matrix-assisted laser desorption/ionization time-of-flight mass spectrometry, Rapid Commun Mass Sp. **22** (2008) 2779-2790.
28. I. Fournier, C. Marinach, J.C. Tabet, G. Bolbach, Irradiation effects in MALDI, ablation, ion production, and surface modifications. PART II: 2,5-dihydroxybenzoic acid monocrystals, J Am Soc Mass Spectr. **14** (2003) 893-899.
29. M. Wiegelmann, J. Soltwisch, T.W. Jaskolla, K. Dreisewerd, Matching the laser wavelength to the absorption properties of matrices increases the ion yield in UV-MALDI mass spectrometry, Anal Bioanal Chem. **405** (2013) 6925-6932.

30. A. Koubenakis, V. Frankevich, J. Zhang, R. Zenobi, Time-resolved surface temperature measurement of MALDI matrices under pulsed UV laser irradiation, The Journal of Physical Chemistry A. **108** (2004) 2405-2410.
31. T. Hoyer, W. Tuszynski, C. Lienau, Ultrafast photodimerization dynamics in α-cyano-4-hydroxycinnamic and sinapinic acid crystals, Chemical physics letters. **443** (2007) 107-112.
32. F. Brygo, A. Semerok, R. Oltra, J.-M. Weulersse, S. Fomichev, Laser heating and ablation at high repetition rate in thermal confinement regime, Appl Surf Sci. **252** (2006) 8314-8318.